Contrib Mineral Petrol
DOI 10.1007/s00410-006-0140-1

ORIGINAL PAPER

The last lavas erupted during the main phase of the Siberian flood volcanic province: results from experimental petrology

Linda T. Elkins-Tanton · David S. Draper · Carl B. Agee · Jessica Jewell · Andrew Thorpe · P. C. Hess

Received: 9 February 2006 / Accepted: 21 August 2006

Abstract The final lavas of the Siberian flood basalts are a ~1,000 m thick section of meimechites, high-alkali, high-titanium, hydrous lavas that contrast sharply with the tholeiites that precede them. This paper presents a phase equilibrium study indicating that a candidate primary meimechite magma with 1 wt% water originated at ~5.5 GPa and 1,700°C, both hotter and shallower than other estimates for melting beneath continental lithosphere. The experiments also suggest that a higher volatile content was involved in meimechite source genesis. Both the absence of orthopyroxene in any experiment and the close field association with carbonatites suggest that the meimechite source region may have been metasomatized with a CO_2-rich fluid. A small additional quantity of CO_2 and water would move magma origination to ~1,550–1,600°C.

Keywords Meimechite · Siberian flood basalt · Carbon dioxide · Experimental petrology · Multiple saturation

Communicated by T.L. Grove.

L. T. Elkins-Tanton (✉) · J. Jewell · A. Thorpe · P. C. Hess
Department of Geological Sciences, Brown University,
324 Brook St, Providence, RI 02912, USA
e-mail: Linda_Elkins_Tanton@brown.edu

D. S. Draper · C. B. Agee
Institute of Meteoritics, University of New Mexico,
Albuquerque MSC03 2050, NM 87131-0001, USA

Introduction

The Siberian flood basalt province is the largest continental flood basalt in the rock record, with volume estimated between 2 and 5×10^6 km^3 (Milanovskiy 1976; Masaitis 1983; Renne and Basu 1991; Reichow et al. 2002; Saunders et al. 2005; though Dobretsov and Vernikovsky (2001) estimated a volume of $3–4 \times 10^7$ km^3 including intrusives). The eruptions were apparently coincident with the end-Permian extinction, the largest extinction in Earth history (Kamo et al. 2003). If this relationship is causal it is a critical link between the evolution of the Earth and the evolution of life on Earth. Causation has not been demonstrated, though a wide range of possible mechanisms have been suggested. One notable possibility is that carbon dioxide and sulfur emitted from the lava triggered global climate change sufficient to initiate extinctions (Campbell et al. 1992).

Most of the volume of the Siberian flood basalts consists of high- and low-titanium picrites and basalts lacking primary hydrous minerals (Fedorenko et al. 1996). The province also contains about 10% interbedded mafic volcaniclastic deposits (Fedorenko et al. 1996), and is underlain by up to 700-m thick sequence of volcaniclastic deposits. This vast underlying deposit may constitute as much as ~25% of the volume of volcanic rocks (Ross et al. 2005). The proportion of volcaniclastics is significantly higher in Siberia than in other flood basalt provinces. The final magmas of the main flood basalt event, the focus of this study, show additional evidence for volatile involvement.

These final magmas of the main Siberian flood volcanic event are a suite of rocks found in the Maymecha-Kotuy region of Siberia, about 500 km east

of Noril'sk, site of the most studied section of the basalts. Fedorenko and Czamanske (1997) report that this 70,000 km^2 province is the only one in the world where high-Ti, alkaline, ultramafic rocks predominate over basalts. A large portion of these rocks form the type locality for meimechites, which are defined by the IUGS as rocks with between 36 and 52 wt% SiO_2 and more than 18 wt% MgO (Fig. 1).

Kamo et al. (2003) states that U–Pb dates of the lowermost units in the Maymecha-Kotuy region have ages of 251.7 ± 0.4 Ma (this sample was from the Arydzhangsky suite, equivalent to the mid- to lowermost units in the Noril'sk area), and the near-uppermost unit of 251.1 ± 0.3 Ma, implying that the entire 6,500 m sequence of the Siberian flood volcanic province was produced in less than one million years. The intrusions in the Noril'sk area of the Siberian flood basalts date to 251.2 ± 0.3 Ma (Kamo et al. 1996), demonstrating that the Maymecha units are the last voluminous mafic magmatism of the event, though smaller volcanic events continued in the Taimyr, the West Siberian Basin, and the Kansk-Taseevskaya Basin for about 20 Myr (Kazanskii et al. 2000; Walderhaug et al. 2005; Ivanov et al. 2005).

Though these unusual and important rocks have been widely reported on in the Russian literature, little of that literature has been translated to English. Recent studies in English include Sobolev et al. (1991), Arndt et al. (1995, 1998), and Fedorenko and Czamanske (1997). These studies have focused on reporting compositions and petrology of meimechite samples and modeling their possible parental magmas and petrogenesis. In this study, we report compositions of three new meimechite samples, but primarily we present the results of an experimental phase diagram study of the most likely primary meimechite melt, indicating its pressure and temperature of origin as well as the composition of the source that melted to create these rocks.

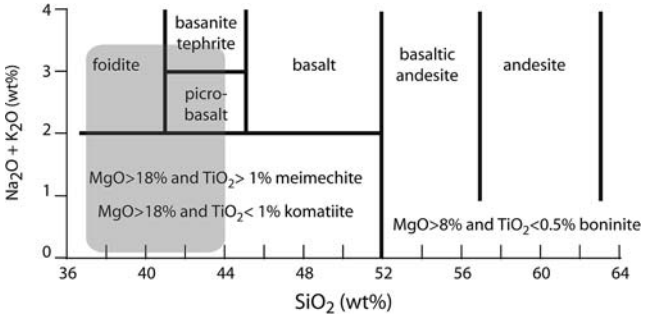

Fig. 1 Revised IUGS classification of high-Mg volcanic rocks, after Le Bas (2000). *Shaded area* indicates the compositional range of rocks in the meimechite section of the Maymecha-Kotuy province of the Siberian flood basalts

Petrology of the Maymecha-Kotuy

The Siberian flood volcanic sequence in the Maymecha-Kotuy region is about 4,000 m thick (Fedorenko and Czamanske 1997). Mapping in this area began in 1937; for a review of the history of research in this area see Fedorenko and Czamanske (1997). Of the ~4,000 m sequence, about 3,000 m are younger rocks than are found in the Noril'sk section, the most studied of the Siberian flood basalt sections. These young rocks [ca. 251.1 Mybp (Kamo et al. 2003)] are among the youngest known extrusive rocks of the Siberian flood volcanics (Fedorenko and Czamanske 1997; Kamo et al. 2003; Ivanov et al. 2005).

The sequence at Maymecha-Kotuy begins with a basaltic tuff unit, followed by a diverse suite of alternating low-Ti and high-Ti lavas, and completed by the 1,400 m thick Maymechinsky suite (Fedorenko and Czamanske 1997). This suite begins with ~400 m of porphyritic picrites and limburgites, and ends with ~1,000 m of meimechites (here we use the IUGS accepted spelling of the Russian word).

Meimechites appear to have lower $^3He/^4He$ ratios than do the rest of the Siberian flood basalts. Basu et al. (1995) reports that analyzed meimechites have $^3He/^4He$ ratios from 2.4 to 5.0, while other rocks from the Siberian flood basalts have $^3He/^4He$ ratios as high as 12.7, thought to be indicators of a deep, undegassed source. Similarly, the meimechites have ε_{Nd} values from 2 to 5.3, far higher than the 0–2.6 found in other members of the Siberian flood basalts (Basu et al. 1995; Arndt et al. 1998). Kogarko and Ryabchikov (1995) report even higher ε_{Nd} for meimechites, from 4.8 to 6.0. Meimechites are highly enriched in incompatible elements, but lack the negative Nb–Ta and Ti anomalies associated with continental lithosphere (Arndt et al. 1995). Their trace and isotopic characteristics are therefore consistent with an enriched source comparable to those of ocean island basalts, such as a metasomatized sub-lithospheric mantle source, and differing significantly from the remainder of the volcanic rocks in the Siberian province (Arndt et al. 1998; Carlson et al. 2006).

Compositionally, meimechites are similar to group I kimberlites, with higher incompatible element concentrations and associations with mica (Francis 1995, 2003). Meimechite provenance, therefore, may be distinct from that of the basalts that make up the bulk of the flood basalt province (Fig. 2) (e.g., Sheinmann 1947; Sobolev and Slutskii 1984; Francis 1995). The

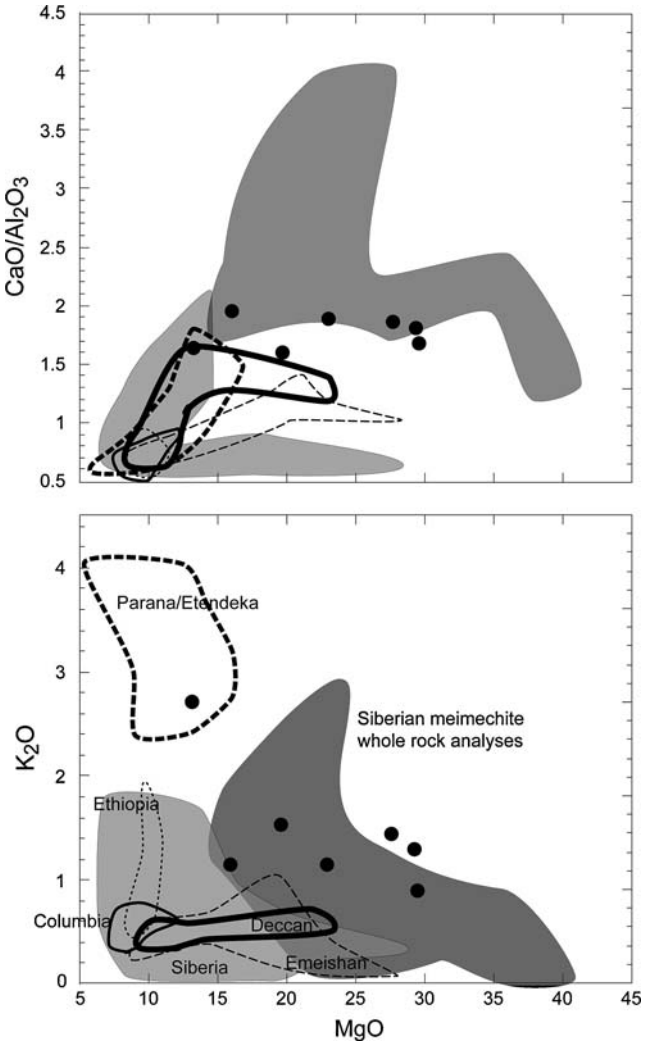

Fig. 2 Flood basalt major element comparisons. Siberian flood basalt main sequence in *light grey*, meimechite whole rock analyses in *dark grey*, meimechite melt inclusions as *filled circles*. Other provinces as labeled in lower diagram. Although they lie conformably directly above the rest of the Siberian flood basalts, the meimechites have distinct compositions. To avoid the majority of the effects of fractionation, only compositions with Mg#s above 60 are included. Data from Sobolev et al. (1991), Fedorenko and Czamanske (1997), Zolotukhin and Allmukhamedov (1991), Arndt et al. (1995), Wooden et al. (1993), Fedorenko et al. (1996), Zolotukhin and Al'Mukhamedov (1988), Ryabov et al. (1985), Dalrymple et al. (1995), Lightfood et al. (1990), Hawkesworth et al. (1995), Hooper and Hawkesworth (1993), Beane et al. 1988), Mahoney et al. (1985), Chung and Jahn (1995), Xu et al. (2001), Stewart and Rogers (1996), Mohr and Zanetton (1988), Piccirillo (1988) and Gibson et al. (1999)

rocks of the Maymecha-Kotuy province are closely associated with the 2,000 km^2 Guli intrusive-volcanic complex of ankaratites, meimechites, dunites, and pyroxenites and two carbonatite bodies that lies just to the east of the Maymecha-Kotuy province (Fedorenko and Czamanske 1997). The dunites are suggested to be the cumulate fractionates from the magma parental to the carbonatites (e.g., Sheinmann 1947; Sobolev and Slutskii 1984), and thus it is possible that all the rocks may be linked in a mutual high-CO_2 provenance. The Guli complex, however, is slightly younger than the meimechites: Kamo et al. (2003) reports an age of 250.2 ± 0.3 Ma. Meimechites also had some pre-eruptive water and likely fluorine content: samples have been found with primary biotite in their groundmass (Arndt et al. 1995; Fedorenko and Czamanske 1997).

Based on petrologic modeling, several researchers have made estimates of the pressure and temperature of meimechite genesis. Sobelev et al. (1991) concluded that meimechites originated at 230–300 km depth and a temperature of 1,800–1,900°C. Through study of trace-element concentrations, Arndt et al. (1995) concluded that the magma must have been the result of either ~1% melt of a primitive mantle source or ~7% melt of an enriched source produced at 8–10 GPa. Arndt et al. (1998) concluded similarly that the meimechites were the result of low degrees of melting (<7%) at depths of 250–300 km, and the variety of magmas in the region were the result of melting discrete mantle sources that were erupted through separate plumbing systems. Kogarko and Ryabchikov (1995), in contrast, concluded from their modeling efforts that the meimechites must be the result of melting by ~4% a portion of the mantle lithosphere that had been metasomatized by melt from an earlier event. This enriched lithosphere was thought to have melted at 5 GPa and about 1,800°C. They also noted, importantly, that meimechites are similar to kimberlites but appear to have had a lower primary CO_2 content, perhaps because the meimechites originate in regions with thinner lithosphere, where carbon solubility is therefore lower. The question remaining from the Kogarko and Ryabchikov (1995) study is the source of the extreme temperatures.

Finding the meimechite primary liquid

Because the purpose of this experimental study is to determine the mantle melting conditions and compositions that lead to the production of Siberian meimechites, it is first necessary to ensure that the starting composition used is as close to a primary mantle melt as possible. The goal of this study is to find the pressure and temperature of multiple saturation, that is, the point on the liquidus of this composition at which a mantle-like assemblage of minerals exists. If the experimental composition is that of a primary mantle melt and it is returned to the temperature and pressure of its origination, then a small drop in temperature should cause it to crystallize the phases

with which it last equilibrated. At other points along the liquidus, only one or two mineral phases will crystallize.

The mineral assemblage at multiple saturation generally is interpreted as the residue that was left behind at the time of melt segregation. If the magma is the result of adiabatic decompression over a pressure range, then the multiple saturation temperature and pressure are interpreted as the average of the decompression path. If the magma was not primary, then it may be multiply saturated with the phases that fractionated on its journey from source region to site of eruption (again assuming that only fractionation has occurred and no interaction occurred with surrounding or mixing with other magmas).

The major element trends of the bulk compositions of meimechites are consistent with addition and subtraction of only olivine, as noted by other researchers (Fig. 3, and see Arndt et al. 1995). Olivine is the common phenocryst in meimechites. The trend to high MgO-content meimechites can be made by adding the liquidus olivine of a mid-trend composition, as shown in Fig. 3a, c, but not with liquidus olivines from less or more magnesian bulk compositions. This line of reasoning leads to the conclusion that the meimechite primary liquid lies near that mid-trend composition.

One reasonable starting point for identifying a bulk rock as a primary liquid composition is to test its composition for equilibrium with its own olivine xenocrysts, and for equilibrium with mantle olivine, expected to have a forsterite content that lies within the range of 89–93. Compositions of the cores of olivine phenocrysts from meimechites are compared to the bulk compositions of the whole rocks to test for equilibrium (Fig. 4). Assuming that the olivine cores were the first to crystallize from the bulk rock when it was a liquid, they should be in Fe–Mg exchange equilibrium with the bulk rock, as defined by a K_D, where $K_D = \text{wt\%}[(Fe^{xtl}/Mg^{xtl})/(Fe^{liq}/Mg^{liq})]$.

Here we consider olivine-bulk rock K_Ds between 0.30 and 0.34 [Herzberg and O'Hara (2002) demonstrated that K_D often rises with MgO content to values above a nominal 0.30–0.32 value]. Rocks that lie to the right of the proposed K_D lines have experienced olivine addition, and those to the left have lost olivine. The olivine core analyses indicate that meimechites with bulk rock Mg#s between at most Mg# 73 and 78 are candidates to have been liquids [where Mg# = molar (Mg/(Mg+Fe))]. Meimechites with Mg#s in this range contain between 22 and 29 wt% MgO.

In the absence of glassy lavas, melt inclusions are often the closest available material to a primary melt. Ten olivine-hosted meimechitic melt inclusions were measured and reported in Sobolev et al. (1991). These melt inclusions have markedly higher alkali content than do the meimechite whole rock compositions, almost certainly reflecting alkali loss from whole rocks during the post-magmatic hydrous alteration event. A very few meimechite whole rock analyses also contain high alkalis, although these are at the low end of MgO content.

Because compositions with higher MgO than predicted liquid compositions are obtained through olivine addition, these compositions should not be found in melt inclusions. The melt inclusion data available from Sobolev et al. (1991) (Fig. 3b, c) extends just past the region of candidate liquid compositions.

Arndt et al. (1995) concluded that the meimechite primary magma had MgO from 25 to 27 wt%, ~1,000 ppm NiO, and 2,000 ppm Cr_2O_3, in agreement with the findings here. Sobolev et al. (1991), however, concluded that the primary magma had as much as 29 wt% MgO. Based on the analyses presented here and those from Arndt et al. (1995), we prefer a primary composition with 25–27 wt% MgO. The most likely primary liquid composition based on these arguments, melt inclusion 2 from Sobolev et al. (1991) (S2 in Table 1), is chosen as the experimental composition.

Experimental and analytic techniques

Preparing a experimental starting material

A synthetic analog of the chosen starting composition was made using the following high-purity oxides: SiO_2, MgO, Fe_2O_3, $CaCO_3$, Al_2O_3, TiO_2, K_2CO_3, NaCl, and $CaHPO_4$. The powder, called SYNS2, was ground in an agate mortar under ethanol for 1.5 h, and then conditioned for 3 h in a gas-mixing furnace at 940°C, sufficient for decarbonation, with oxygen fugacity corresponding to the quartz–fayalite–magnetite buffer. The final bulk composition was checked through analyses of glass in multi-anvil experiments above the liquidus, and is presented in Table 1 and in Fig. 3b, c. Because the powder is hydrophilic (believed to be caused in large part by the use of MgO powder) it retained water even after conditioning. The water content of the conditioned experimental mix was measured through difference of electron microprobe analyses from 100% in glass analyses from multi-anvil experiments. In no case was the water content inferred from this process less than 1 wt%, and in some measurements it was as high as 2 wt%; no glass analyses yielded totals above 100%. Quench material concentrates water in the remaining unaltered glass, and the

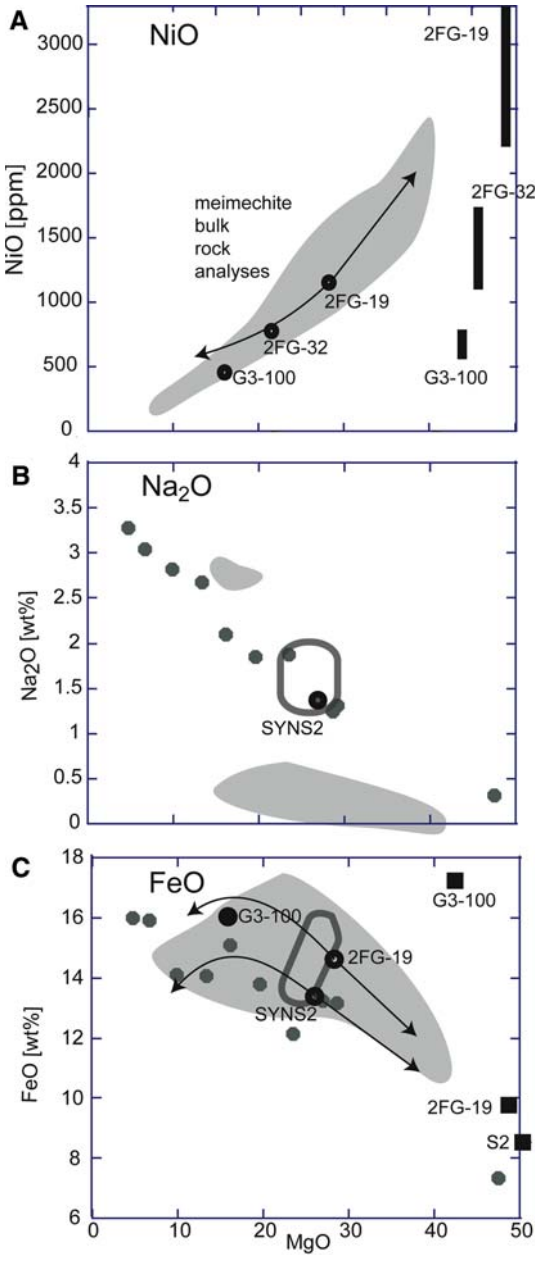

◄ **Fig. 3** Major element diagrams for meimechites, meimechite melt inclusions, and associated picrites and basalts. Data delineating meimechite bulk compositions field from Arndt et al. (1995), Fedorenko and Czamanske (1997), Zolotukhin and Allmukhamedov (1991). *Filled circles* meimechite olivine melt inclusion compositions from Sobolev et al. (1991). **a** NiO versus MgO: *arrows* indicate 50% liquidus olivine addition and 50% olivine fractionation from a melt of the composition 2FG-19 (from Fedorenko and Czamanske 1997). *Black bars* show possible liquidus olivine compositions given a range of reasonable NiO distribution coefficients between olivine and melt. Meimechite trend is consistent with addition of liquidus olivine from a melt of composition 2FG-19, but not from less magnesian bulk compositions. **b** Na_2O versus MgO: melt inclusion data contains far higher alkalis than meimechite bulk compositions. Range of possible liquid compositions from olivine Mg# analysis (Fig. 4) outlined by the *grey circle*. Experimental composition SYNS2 is shown with *dark symbol*. **c** FeO versus MgO: *symbols* as in parts **a** and **b**. Liquidus olivine compositions (*black squares*) for bulk rock 2FG-19 and experimental starting composition SYNS2 are both consistent with the trend of meimechite compositions, but the less magnesian composition G3-100 (from Fedorenko and Czamanske 1997) cannot recreate the trends

analyses with higher water by difference came from experiments with some quench growth. The experimental starting material is inferred to contain ~1 wt% water, though its water content can only be said with assurance to lie between 1 and 2%. Material from a single batch of conditioned SYNS2 was used for all the one-atmosphere, piston-cylinder, and multi-anvil experiments described here.

One-atmosphere experiments

One-atmosphere experiments were conducted in Mac Rutherford's laboratory at Brown University. Powdered starting material was wrapped in molybdenum foil and sealed in an evacuated silica tube using a vacuum pump and an acetylene welder's torch. The silica tubes were hung by wire in the furnace's hot spot for between 1 and 2 h; experiments were conducted over the temperature interval 1,230–1,450°C. The tubes were lifted from the furnace by their hanging wires and quenched in water. The experimental products were unwrapped from the molybdenum foil, mounted in epoxy on microscope slides, and polished for both optical and electron microprobe analysis.

Piston-cylinder experiments

Piston-cylinder experiments were conducted in Yan Liang's laboratory at Brown University in a Walker-style 3/4-in. diameter piston-cylinder apparatus calibrated to the melting temperature of NaCl at 1 GPa. Experiments on the synthetic starting material were conducted at 1.0 GPa (corresponding to about 33 km depth) and at temperatures from 1,350 to 1,600°C. For each experiment ~10 mg of conditioned starting material was packed into a 6 mm-high graphite crucible and capped with a press-fit graphite lid. The capsule was then placed inside an MgO sleeve and powdered graphite was packed around it. The assembly was positioned in the hot spot of a graphite heater using MgO spacers, with a pyrex outer sleeve and salt as the pressure medium. No pressure correction was needed.

Experiments in the piston-cylinder apparatus were pressurized to 0.8 GPa, heated at 75°C/min to 1,000°C where the temperature was maintained for 6 min, then heated to the desired experimental temperature at a

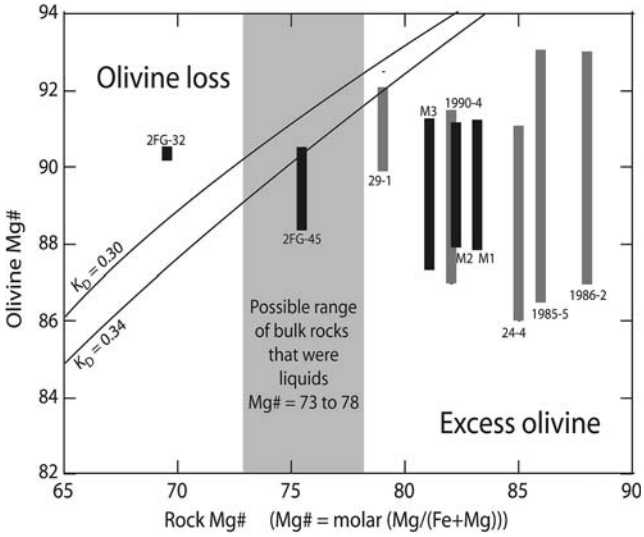

Fig. 4 Olivine core Mg#s versus bulk rock Mg# for natural meimechites. Rocks with olivine cores lying near a K_D of 0.3–0.34 with respect to their bulk rock composition are candidates to have been liquids without later loss or gain of olivines. Data in *black* from this study, and in *grey* from Arndt et al. (1995)

rate of 100°C/min, and then brought to final run pressure. Temperatures were measured and controlled using a tungsten–rhenium thermocouple in a four-bore alumina thermocouple insulator inserted to within 1 mm of the graphite capsule, but separated from it by an MgO spacer. A 20°C temperature correction was made between the thermocouple junction and the experimental charge. Experiments were maintained at pressure and temperature for between 0.5 and 3.3 h.

In an attempt to obtain crystal-free glass the experiments were temperature- and pressure-quenched by shutting off the power to the furnace and simultaneously dropping the pressure to 0.8 GPa. The fastest cooling required about 15 s to reach 500°C, and was never sufficient to prevent growth of quench olivine crystals in the glass phase. In previous experimental studies, even those with high Mg# starting materials, this ''pressure-quenching'' technique was successful (see Elkins-Tanton and Grove 2003; Elkins-Tanton et al. 2003). In the case of this starting material, we suspect that the combination of high MgO and high alkali content reduced viscosity to the point that cleanly quenching to glass in a 3/4-in. piston-cylinder is impossible. Following quenching, all the experimental charges were sawn in half vertically, mounted in 1 in. epoxy disks, polished, and carbon-coated.

Multi-anvil experiments

To reach the multiple saturation point of meimechite pressures and temperatures are required that extend beyond the range available in a piston-cylinder apparatus. Multi-anvil experiments spanning pressures from 3.0 to 6.5 GPa and temperatures from 1,500 to 1,850°C were conducted at the Institute of Meteoritics, University of New Mexico. The apparatus is calibrated to both the quartz–coesite and coesite–stishovite transitions. Synthetic starting material was loaded into a graphite capsule with a press-fit graphite lid and positioned in cast, finned octahedra of Aremvo Ceramavast©ceramic that had been fired at 1,100°C prior to being drilled for sample assembly, and then stored at 110°C in a drying oven until ready for use. Procedures and calibrations for the multi-anvil are as described in Agee et al. (1995). The graphite capsules were placed inside alumina rings and positioned in the center of rhenium foil heaters using crushable alumina spacers.

Temperatures were measured at the rhenium foil heater using radially-inserted W/Re thermocouples, and controlled by a Eurotherm 930P programmable controller. Experiments were pressurized to 1 GPa, then heated to 100°C, then pressurized to 2 GPa, then heated to 500°C, and similarly stepped to final pressure and temperature over approximately 40 min. Experiments were quenched by turning off power to the heater, which because of the high thermal mass of the cool parts of the multi-anvil apparatus allows sample temperatures to fall from temperatures as high as 1,700°C to below the glass transition temperature of about 600°C in less than 2 s. This cooling rate is sufficient to quench to analyzable glass in many experiments.

Analysis of natural samples and experimental products

Analyses were performed on experimental products and natural samples both at Brown University on a Cameca SX100 microprobe, and on a JEOL-JXA-733 Superprobe at MIT. At Brown, a 1-μm spot with a 15 nA beam and an accelerating voltage of 15 kV was used to analyze phases, following normal probe standardization procedures. At MIT, a 1-μm spot size with a 10 nA beam current and an accelerating voltage of 15 kV was used to analyze phases, following standardization. Analyses on the same phases (mineral and glass) by the two probes usually agree within one standard deviation and always within two standard deviations.

Bulk analyses of pressed powder pellets of the three meimechite samples from the American Museum of Natural History were performed by Michael Rhodes at the Ronald B. Gilmore XRF Laboratory at the University of Massachusetts at Amherst by X-ray fluorescence using a Siemens MRS-400 multi-channel

Table 1 Bulk compositions in oxide wt% or ppm for American Museum of Natural History meimechites M1, M2, and M3, melt inclusion#2 from Sobolev et al. (1991), and the synthetic starting composition used in experiments

Sample	M1	M2	M3	S2	SYNS2
N	2	2	2		
SiO_2	40.97247	41.30049	41.34472	40.19	40.23
TiO_2	1.9269	2.49312	2.6010.3	3.55	3.43
Al_2O_3	2.19227	2.92116	2.99621	4.49	4.61
FeO*	12.82191	12.91630	13.37041	13.27	12.86
MnO	0.2101	0.2133	0.2155	0	0
MgO	36.01239	33.33359	32.35228	26.92	26.69
CaO	5.29721	6.19411	6.48715	8.16	7.95
Na_2O	0.24598	0.15569	0.17076	1.30	1.04
K_2O	0.0832	0.1371	0.1234	1.48	1.39
P_2O_5	0.2416	0.3414	0.3425	0.63	0.85
H_2O		nm	nm		1.0
Total	100.00	100.00	100.00	100.00	100.00
Total*	98.9	98.9	99.0		
Mg#	83.4	82.1	81.2	78.3	78.7
				Error (%)	
Nb (ppm)	31.4	41.0	40.3	3.7	
Zr (ppm)	142	187	198	6.7	
Y (ppm)	8.7	11.2	11.6	2.0	
Sr (ppm)	250	363	386	1.6	
U (ppm)	0	0	0		
Rb (ppm)	2.6	4.4	3.9	0.0	
Th (ppm)	3	3	4		
Pb (ppm)	2	2	2	50.0	
Ga (ppm)	6	8	8	0.0	
Zn (ppm)	95	94	92	0.9	
Ni (ppm)	1823	1656	1556	9.6	
Cr (ppm)	3356	2629	2773	5.0	
V (ppm)	133	167	161	3.7	
Ce (ppm)	59	79	81	12.2	
Ba (ppm)	167	211	218	5.3	
La (ppm)	25	34	34	6.7	
Ti (wt%)	1.89	2.35	2.44	4.5	

Reported values are average of *N* analyses. Oxides are renormalized to 100%, and total with an asterisk is the total before renormalization. Deviation from 100% in original total can be interpreted as water content. Label ''nm'' indicates the oxide was not measured. Beneath major elements two standard deviations on their average are given, in units of the last significant digit of the oxide wt%. Errors in trace element analyses are from analyses of known USGS standard BVHO-1, analyzed at the time of the unknown meimechites

spectrometer. Trace element contents of these samples were performed similarly in a Phillips PW2400 sequential spectrometer.

Results

New meimechite whole-rock analyses

Three new meimechite samples (M1, M2, and M3 collected from the Maymechinsky formation by Valeri Fedorenko for the American Museum of Natural History) were examined in thin section and analyzed for bulk composition. All natural phase analyses are reported in Table 2.

All samples contain chromite-bearing olivine phenocrysts up to 6 mm in length (Fig. 5) set in a groundmass of serpentinized glass, clinopyroxene, spinels showing variable solid solution between titanomagnetite and ülvospinel, and occasional grains of apatite (Fig. 6). Sample M2 also contains groundmass olivine, and sample M1 contains spinel phenocrysts as well as smaller groundmass spinel. None of the samples contain any hydrous minerals, such as the biotite reported by Arndt et al. (1995).

Both the serpentinized glass and veins of serpentine containing grains of magnetite in the olivine phenocrysts are evidence for extensive post-magmatic alteration. As noted by previous investigators (e.g., Sobolev and Slutskii 1984), both interstitial glass and groundmass olivine are largely to completely serpentinized.

In addition to the new samples from the American Museum, phases from two samples previously reported in Fedorenko and Czamanske (1997) were analyzed in a microprobe from thin sections. Sample 2FG-32 contains groundmass clinopyroxene that ranges in Mg# from 77.6 to 83.4, with CaO contents between 21.5 and 23.7 wt%.

The olivine phenocrysts are remarkably homogeneous. Although there is a relatively consistent decline in MgO content in the olivine phenocrysts from core to rim, the range is only from 50.0 to 49.3 wt% MgO (Fig. 7). Olivine–chromite thermobarometry using the QUILF method (Anderson et al. 1993) indicates crystallization at ~1,000°C and 1 kbar.

Experiments

The 15 multi-anvil experiments, 6 piston-cylinder experiments, and 10 one-atmosphere experiments locate a multiple saturation point with olivine, low-calcium clinopyroxene, and garnet on the liquidus at ~5.5 GPa (~175 km depth) at 1,700°C (Figs. 8, 9). Olivine is the liquidus phase at pressures lower than that of the multiple saturation point. No orthopyroxene is present in any experiment at any pressure or temperature.

Table 2 Phases in five natural meimechites analyzed by electron microprobe

Sample	*N*	SiO_2		TiO_2		Al_2O		Cr_2O_3		FeO*		MnO		MgO		CaO		Na_2O		NiO		ZnO	Total	Mg#
M1																								
Olivine phenocryst (high Mg#)	1	40.59		0.05		0.04		0.08		8.65		0.17		50.14		0.41		nd		0.40		nd	100.53	91.17
Olivine phenocryst (low Mg#)	1	39.99		0.06		0.02		0.05		11.85		0.16		47.93		0.51		nd		0.31		nd	100.88	87.82
Olivine phenocryst (average)	7	40.22	63	0.04	3	0.03	2	0.06	5	10.27	282	0.16	4	49.15	241	0.45	1	nd		0.39	8	nd	100.77	89.51
Spinel (in olivine, low Cr)	1	0.06		6.53		5.62		30.62		44.35		0.35		9.70		0.00		nd		0.27		0.07	97.57	
Spinel (in olivine, high Cr)	1	0.04		4.18		6.51		49.45		24.85		0.21		14.40		0.00		nd		0.23		0.01	99.88	
Clinopyroxene (groundmass)	4	50.58	92	1.90	30	2.07	55	0.25	28	6.13	36	0.08	1	15.71	63	23.28	29	0.39	5	nd		nd	100.39	82.04
Spinel (groundmass, low Ti)	1	0.19		11.09		1.95		2.13		77.27		0.72		0.86		0.15		nd		0.38		0.08	94.82	
Spinel (groundmass, high Ti)	1	0.08		20.75		1.36		1.03		68.99		1.25		1.15		0.10		nd		0.38		0.13	95.22	
Spinel (groundmass, high Cr)	1	0.07		17.15		2.56		6.68		66.61		2.21		1.01		0.07		nd		0.19		0.19	96.74	
Spinel (phenocryst, low Ti)	1	0.02		6.62		5.41		34.54		43.24		0.47		8.18		0.00		nd		0.10		0.11	98.69	
Spinel (phenocryst, high Cr/Ti)	1	0.05		17.52		2.79		5.14		66.85		1.71		2.26		0.08		nd		0.21		0.12	96.73	
Serpentine from filled vesicle	1	41.95		0.09		1.84		0.00		3.27		0.05		38.95		0.15		0.00		0.09		nd	86.47	
M2																								
Olivine phenocryst (low Mg#)	1	39.50		nd		0.01		0.04		11.38		0.25		46.57		0.54		nd		0.26		nd	98.55	87.94
Olivine phenocryst (high Mg#)	1	40.39		nd		0.04		0.1		8.52		0.14		49.24		0.39		nd		0.36		nd	99.18	91.15
Olivine phenocryst (average)	10	39.99	85	nd		0.03	2	0.07	4	9.98	265	0.18	8	48.13	246	0.45	16	nd		0.34	7	nd	99.17	89.58
M3																								
Olivine phenocryst (low Mg#)	1	39.34		nd		0.03		0.06		12.04		0.2		46.94		0.41		nd		0.38		nd	99.40	87.42
Olivine phenocryst (high Mg#)	1	40.57		nd		0.04		0.09		8.54		0.15		49.38		0.43		nd		0.28		nd	99.48	91.15
Olivine phenocryst (average)	9	40.33	140	nd		0.05	3	0.08	3	9.69	271	0.17	6	48.73	215	0.41	10	nd		0.36	8	nd	99.82	89.96
2FG-32																								
Olivine phenocryst (average)	22	40.48	53	nd		nd		0.12	2	9.53	15	0.15	3	49.65	39	0.29	4	nd		0.43	4	nd	100.65	90.28
Chromite (in olivine)	10	nd		3.07	268	3.25	27	56.70	579	21.79	260	0		13.09	63	nd		nd		nd		nd	97.90	
Clinopyroxene (low Mg#)	1	47.33		3.37		4.10		0.07		6.90		0.10		13.45		23.25		0.58		nd		nd	99.15	77.65
Clinopyroxene (high Mg#)	1	50.23		1.99		2.51		0.64		5.35		0.14		15.09		23.64		0.37		nd		nd	99.96	83.41
Clinopyroxene (average)	17	49.45	261	2.66	128	2.94	180	0.14	35	6.39	98	0.14	6	14.75	184	22.92	137	0.46	29	nd		nd	99.85	80.45
Spinel (groundmass, low Ti)	1	nd		17.36		0.94		0.26		73.40		0.28		0.42		nd		nd		nd		nd	92.66	
Spinel (groundmass, high Ti)	1	nd		41.10		0.26		0.05		47.60		1.43		3.47		nd		nd		nd		nd	93.91	
2FG-45																								
Olivine phenocryst (low Mg#)	1	40.09		nd		nd		0.06		11.26		0.20		48.32		0.50		nd		0.38		nd	100.81	88.44
Olivine phenocryst (high Mg#)	1	40.46		nd		nd		0.08		9.08		0.15		50.05		0.44		nd		0.37		nd	100.63	90.76
Olivine phenocryst (average)	37	40.36	36	nd		nd		0.07	4	10.42	155	0.20	6	48.95	135	0.43	11	nd		0.37	5	nd	100.80	89.33
Chromite (in olivine)	5	nd		2.70	42	5.79	17	46.21	74	29.92	152	0		13.53	55	nd		nd		nd		nd	98.15	
Clinopyroxene (low Mg#)	1	44.65		3.81		4.4		0.09		9.99		0.16		13.20		22.1		0.50		nd		nd	98.90	70.19
Clinopyroxene (high Mg#)	1	51.24		1.44		1.67		0.09		5.36		0.10		16.71		22.72		0.33		nd		nd	99.66	84.75
Spinel (groundmass, low Ti)	1	nd		13.56		1.64		0.82		72.25		0.95		5.19		nd		nd		nd		nd	94.41	
Spinel (groundmass, high Ti)	1	nd		47.94		0.21		0.13		39.84		1.03		8.83		nd		nd		nd		nd	97.98	

Reported values are averages of *N* analyses. Major elements in oxide wt% and two standard deviations on their average are given, in units of the last significant digit of the oxide wt%. Mg# is calculated as [molar (MgO/(MgO + FeO))]. The highest and lowest Mg# analyses are given to show the range of compositions. Iron is reported as FeO (spinel analyses do not sum to 100% as a result of reporting all iron as FeO*). Samples M1, M2, and M3 from the American Museum of Natural History and collected by Valeri Fedorenko; samples 2FG-45 and 2FG-32 from Fedorenko and Czamanske (1997) and courtesy of Nick Arndt and Gerry Czamanske

nd not detected

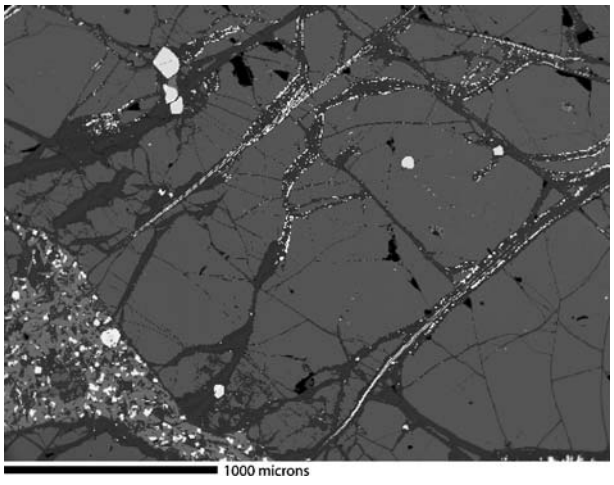

Fig. 5 Backscattered electron photomicrograph of an olivine phenocryst from sample M1. Serpentinized veins show as *darker grey* with tiny bright magnetite grains. *Larger bright* chromites are found in the olivine, while the fine-grained groundmass contains spinels, clinopyroxenes, and serpentinized glass

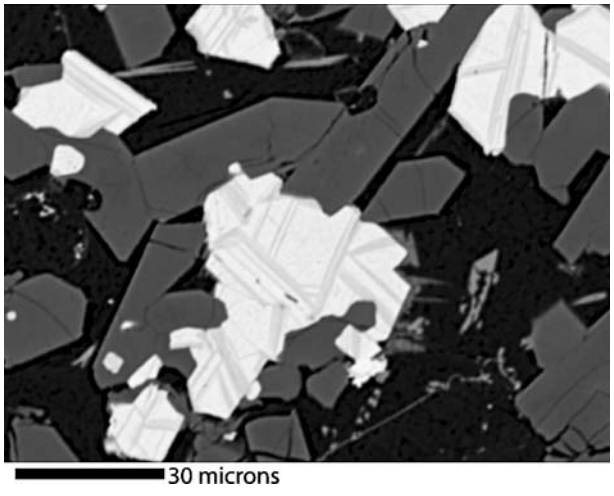

Fig. 6 Backscattered electron photomicrograph of the groundmass of sample M3. *Bright spinels* are intergrown with well-formed clinopyroxenes. The *dark background* is serpentinized glass

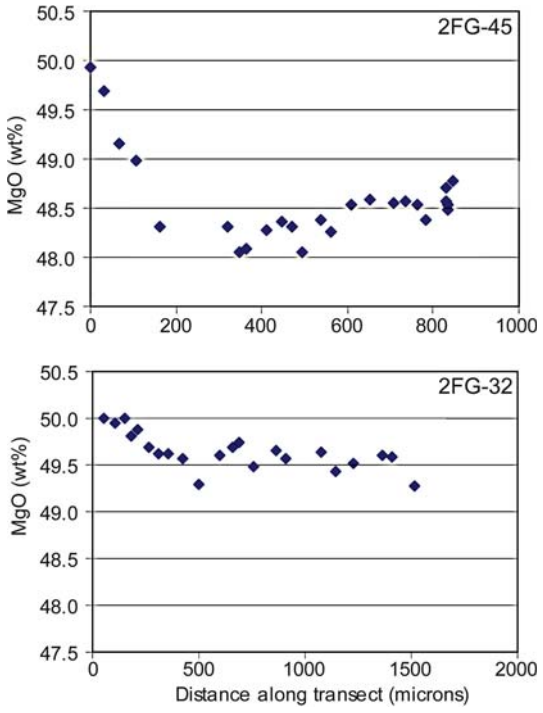

Fig. 7 MgO content of olivine phenocrysts from meimechites 2FG-32 and 2FG-45 showing the relative homogeneity of the large olivines

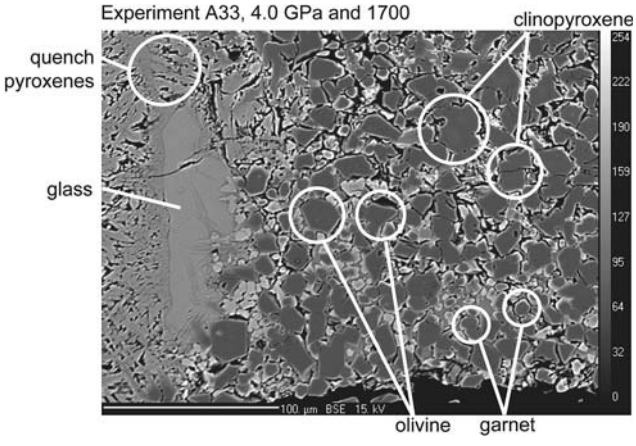

Fig. 8 Backscattered electron photomicrograph of experiment A33 showing multiple saturation with olivine, garnet, and clinopyroxene

The conditions and results of the 15 multi-anvil phase equilibrium experiments for which analyses of multiple phases are available are given in Table 3. No analyses for the piston-cylinder or one-atmosphere experiments are given. The phase relations in these experiments are consistent with those delineated by the multi-anvil experiments, and so they are shown on the phase diagram given in Fig. 9. Glasses in these experiments, however, were universally so quench-modified that no demonstration of mass balance or reasonable Fe–Mg exchange coefficient, K_D, can be shown. The K_Ds in these experiments ranged from 0.18 to 0.28. Only the exceptionally rapid quenching possible in a multi-anvil apparatus made complete experimental analysis possible.

Of the 15 multi-anvil experiments, six contained well-grown homogeneous phases but no analyzable glass due to rapid and pervasive crystal growth during

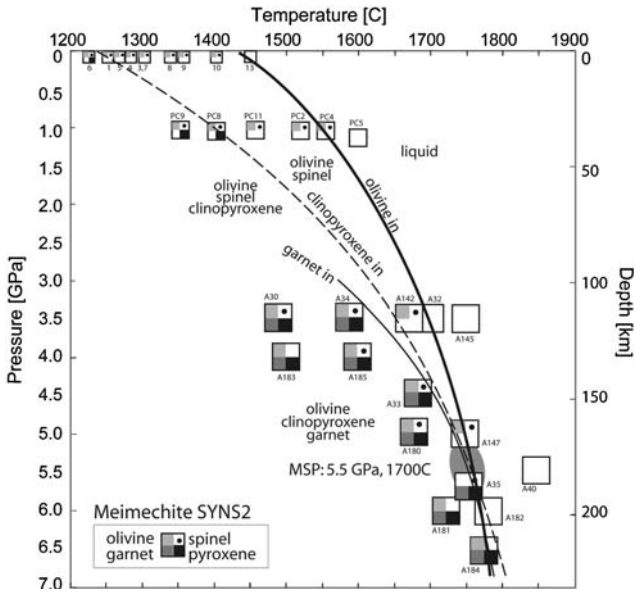

Fig. 9 Phase equilibrium experiments on synthetic analog (SYNS2) of meimechite melt inclusion composition S2 from Sobolev et al. (1991). Experiment numbers are marked. The *filled oval* marks the multiple saturation point. Symbols are approximately the size of errors bounds in P and T. Though glass in experiments at 1 atm and 1 GPa were unanalyzable, phase boundaries are in agreement between pressures

quenching (referred to as quench phases). An additional four experiments were above the liquidus. The remaining five experiments that contained glass free of quench crystals, mass-balanced with the starting composition, and contained well-grown homogeneous phases were used to calculate crystal–liquid exchange equilibria.

While Herzberg and O'Hara (2002) determined a positive relation between olivine-melt K_D and bulk MgO content such that this meimechite experimental composition should have yielded K_Ds between 0.35 and 0.36, the average equilibrium olivine-melt K_D from these experiments is 0.30, and the average clinopyroxene-melt K_D is 0.28. Other experimental projects performed by the authors have yielded equally internally consistent K_Ds, also differing from this study: a dry, high-magnesium lunar compositions yielded average K_Ds of 0.34 to 0.36 (Elkins-Tanton et al. 2003), while a hydrous, alkali-rich, high-magnesium Sierran composition yielded an average K_D of 0.29–0.32 (Elkins-Tanton and Grove 2003). Magnesia content does in general appear to increase olivine-melt K_Ds, but water and alkali content may reduce the K_D, offering an explanation for the relatively low K_D found consistently in this study.

To facilitate analysis of the multi-anvil experiments with multiple phases but no analyzable glass, Fe–Mg exchange coefficients were calculated between pyroxene and olivine as well as between garnet and olivine. Here, $K_D = [X(Fe^{xtl}/XMg^{xtl})/(XFe^{ol}/X\ Mg^{ol})])$. The average equilibrium pyroxene–olivine K_D is 0.95, and the average equilibrium garnet–olivine K_D is 1.74. Experiments with olivine-melt K_Ds far below 0.3 (for example, experiment A182 in Table 3), or pyroxene-melt K_Ds far above 0.3 (for example, experiment A142 in Table 3), can be assumed to be out of equilibrium. The lack of equilibrium shown in a few cases can be assigned to growth of quench crystals. Similarly, consistency of pyroxene–olivine and garnet–olivine K_Ds in the experiments without analyzable glass is some reassurance, in the absence of textural arguments, that those phases are not the result of quench growth. Any phases shown texturally or through K_D values to be quench values are labeled as such in Table 3 and do not appear in Fig. 9.

Discussion

Several pieces of evidence require that meimechites originate from a source substantially different from either the MORB mantle source or hypothetical plume sources, as in the rest of the volcanic province, as has been noted by previous workers (e.g., Sheinmann 1947; Sobolev and Slutskii 1984; Francis 1995, Arndt and Christiansen 1992; Arndt et al. 1995; Fedorenko and Czamanske 1997). First are the enriched trace element signatures, discussed by Arndt et al. (1995, 1998) and Carlson et al. (2006), and the volatile contents of the lavas. New evidence from this study include the lack of orthopyroxene stability at any pressure or temperature studied, and the high temperature relative to the pressure of multiple saturation. These evidences will be discussed separately below.

Evidence for volatile content of meimechite lavas

The temperature obtained at multiple saturation in this study (~1,700°C) is exceptionally high, even for hypothetical mantle plumes. Whole-rock analyses of meimechites show substantial water content through loss on ignition (e.g., Fedorenko and Czamanske 1997). Though this is clearly the result of serpentinization during a post-magmatic product, the reports in Arndt et al. (1995) and Fedorenko and Czamanske (1997) of primary biotite in the groundmass of relatively unaltered meimechites require that the magma erupted with some water content. Magmatic water in meimechites is an indication of a significant tectonic or dynamic change from the melting conditions of the underlying relatively dry magmas. A variety of field

Table 3 Conditions and products of experiments

Run	P	T	t	R^2	Prop.	phase	N	SiO_2		TiO_2		Al_2O_3		FeO		MgO		CaO		Na_2O		K_2O		P_2O_5		Total	K_Ds	K_Ds OL	Mg#
A30	3.5	1,500	0.5	0.16	37	Glass	4	34.34	97	9.31	24	4.66	23	17.34	68	15.01	98	10.73	50	2.43	34	4.15	12	1.96	9	96.93			60.7
				Ti, Na	30	Olivine	5	39.67	45	nd		nd		14.89	32	45.17	42	0.25	4	nd		nd		nd		99.98	0.29		84.4
					26	Pyroxene	5	53.12	86	0.79	15	4.56	90	6.26	28	19.88	97	14.26	76	1.19	10	0.06	3	nd		100.12	0.27	0.96	85.0
					7	Garnet	4	41.22	48	1.74	32	22.56	55	10.12	18	17.91	55	6.40	95	0.07	4	nd		nd		100.02	0.49	1.79	75.9
						Spinel		na																					
						Pyroxene (q)		na																					
A32	3.5	1,700	1.0			Glass (q-modified)	5	42.02	23	4.15	13	5.52	5	14.10	12	20.56	20	10.05	13	1.50	8	1.51	5	0.52	6	97.35			72.2
A33	4.5	1,700	1.0	0.39	49	Glass	3	37.25	43	7.18	4	3.72	8	17.10	69	18.24	33	9.89	21	2.02	34	3.15	13	1.47	3	96.75			65.5
				Ti, Ca	24	Olivine	4	40.01	36	nd		nd		12.89	32	45.87	18	0.24	7	nd		nd		nd		99.01	0.30		86.4
					17	Pyroxene	4	54.11	8	0.51	2	3.31	10	5.72	17	21.58	72	13.06	81	1.08	4	nd		nd		99.37	0.28	0.94	87.1
					9	Garnet	4	41.19	81	2.00	27	22.10	59	8.36	54	20.11	70	6.31	95	0.08	3	nd		nd		100.15	0.44	1.57	81.1
						Spinel		na																					
					1	Pyroxene (q)	4	35.81	186	11.88	179	6.97	97	15.39	88	11.56	273	15.48	207	0.53	22	nd		nd		97.62	1.42		57.2
A34	3.5	1,600	1.0	0.21	49	Glass	3	36.90	58	7.33	47	4.26	13	16.98	20	17.26	87	10.39	18	2.15	33	3.18	7	1.40	33	96.36			64.4
				Ca	25	Olivine	6	39.97	44	nd		nd		13.37	22	45.96	40	0.29	3	nd		nd		nd		99.59	0.30		86.0
					18	Pyroxene	6	53.78	45	0.56	12	3.71	38	6.03	96	21.43	70	13.04	80	1.04	13	nd		nd		99.59	0.29	0.97	86.4
					8	Garnet	4	41.84	38	1.62	30	22.74	27	8.77	38	18.66	55	6.33	60	0.08	3	nd		nd		100.04	0.48	1.67	79.1
						Spinel		na																					
						Pyroxene (q)		na																					
A35	5.6	1,750	1.0			Glass		Unanalyzable: quench growth																					
						Pyroxene	9	55.27	52	0.40	18	2.67	28	6.56	46	24.33	94	9.63	83	1.08	11	0.00		nd		99.94			86.9
						Garnet	4	42.66	48	1.87	42	21.34	46	9.10	27	20.22	64	4.77	57	0.08	4	nd		nd		100.04			79.8
						Spinel		na																					
						Pyroxene (q)		na																					
A40	5.4	1,850	1.0			Glass		Not analyzed																					
A142	3.5	1,650	1.0	0.07	78	Glass	6	40.85	46	4.38	11	6.19	21	13.66	33	20.25	32	10.60	28	1.40	7	1.73	6	1.00	7	96.90			72.5
				Ca	22	Olivine	4	40.02	43	0.06	3	0.13	4	10.46	33	49.28	66	0.30	4	0.04	2	nd		nd		100.29	0.31		89.4
						Pyroxene (q)	6	44.71	54	4.58	21	7.09	23	10.32	95	20.41	62	10.42	103	0.57	8	nd		nd		98.10	0.75	2.38	77.9
A145	3.5	1,750	1.0			Glass	1	40.50		3.69		4.85		13.58		25.65		8.27		1.20		1.41		0.82		99.01			77.1
A147	5.0	1,750	1.0	0.12	85	Glass	6	40.41	46	3.88	8	5.59	15	13.79	55	23.01	47	9.52	23	1.26	10	1.60	6	0.93	4	98.23			74.8
				Fe	15	Olivine	6	40.32	38	0.00		0.20	4	9.52	29	49.07	71	0.27	5	0.00		nd		nd		99.38	0.32		90.2
A180	5.0	1,675	1.0			Glass		Unanalyzable: quench growth																					
						Olivine	5	40.65	36	0.00		0.20	14	10.77	31	48.35	25	0.37	23	0.07	3	nd		nd		100.41			88.9
						Pyroxene	5	54.77	43	0.33	3	3.20	33	4.88	29	22.67	63	13.16	92	0.96	8	0.17	8	nd		100.14		0.97	89.2
						Garnet	3	41.90	62	1.80	35	21.79	66	7.78	3	20.40	93	6.23	79	0.00		0.00		nd		100.16		1.77	82.4
A181	6.0	1,725	1.0			Glass		Unanalyzable: quench growth																					
						Olivine	5	40.53	23	0.06	5	0.15	7	9.90	23	49.24	26	0.24	10	0.00		nd		nd		100.12			89.9
						Pyroxene	5	55.27	59	0.27	4	2.45	11	4.49	54	22.72	81	13.99	124	0.98	14	0.10	5	nd		100.27		0.98	90.0
						Garnet	4	43.11	90	1.49	39	20.47	70	7.40	25	21.86	60	5.49	35	0.00		0.00		nd		100.27		1.71	84.0
A182	6.0	1,775	0.3			Glass	2	41.92	31	4.03	13	5.36	18	13.08	106	24.34	26	8.94	3	1.04	9	0.47	13	0.81	3	97.87			76.8

Table 3 continued

Run	P	T	t	R^2	Prop.	phase	N	SiO_2		TiO_2		Al_2O_3		FeO		MgO		CaO		Na_2O		K_2O		P_2O_5		Total	K_Ds	K_Ds OL	Mg#
						Olivine (q)	2	42.03	44	0.00		0.14	48	6.80	66	52.00	43	0.24	85	nd		nd		nd		101.21	0.24		93.2
						Pyroxene (q)		na																					
						Spinel (q)		na																					
A183	4.0	1,500	1.0			Glass		Unanalyzable: quench growth																					
						Olivine	5	40.20	50	0.12	3	0.13	5	13.81	8	46.28	35	0.35	9	nd		nd		nd		100.89			85.7
						Pyroxene	3	53.01	80	0.73	8	5.32	97	4.97	9	18.60	70	17.39	19	1.05	25	0.10	3	nd		101.17		0.90	87.0
						Garnet	3	40.98	35	2.28	21	21.37	66	9.24	21	18.39	90	8.30	46	0.19	2	0.06	2	nd		100.81		1.88	78.0
A184	6.5	1,775	1.0			Glass		Unanalyzable: quench growth																					
						Olivine	2	41.16	28	0.06	2	0.19	2	8.37	69	50.55	95	0.28	2	nd		nd		nd		100.61			91.5
						Pyroxene	3	52.30	47	1.12	7	4.20	62	3.98	25	23.20	47	14.70	15	1.70	11	0.40	2	nd		101.60		1.04	91.2
						Garnet	2	42.99	16	2.17	10	19.33	20	6.41	21	23.22	37	6.46	30	0.05	2	0.00		0.29	0	100.92		1.61	86.6
A185	4.0	1,600	1.0			Glass		Unanalyzable: quench growth																					
						Olivine	3	39.30	53	0.09	4	0.18	0	11.68	13	47.02	22	0.34	4	0.00		0.00		nd		98.61			87.8
						Pyroxene	3	52.12	61	0.42	3	4.15	42	5.22	36	22.82	49	12.72	4	0.76	65	0.06	1	nd		98.27		0.92	88.6
						Garnet	2	41.36	1	1.84	5	21.85	64	8.49	24	19.65	56	6.47	33	nd		nd		nd		99.66		1.89	80.5

Pressure is GPa, temperature in °C, run times in hours. Sum of squared residuals resulting from multiple linear regression of analyzed phases against starting compositions is given as R^2 , and elements with errors most responsible for the residual are listed. Phase proportions are also the results of linear regression. Phases denoted as "quench" ("q") can be shown both texturally and compositionally to be disequilibrium phases grown rapidly as T and P sank after the experiment is completed; these are not equilibrium phases from the experiment but are shown because of their prominence in the final product. Run product compositions are given in oxide wt%. Glass analyses are renormalized to 100% but the original, unnormalized total is given. Reported values are averages of N analyses. Number after oxide is 2 standard deviations on the average and is in units of the last significant digit of the oxide wt%. Not detected is marked as "nd;" "na" indicated not analyzed for. K_Ds between minerals and glass are given, as are Fe–Mg K_Ds between olivine and other minerals when glass was unanalyzable (see text)

and experimental studies have concluded that fluorine significantly extends the stability range of phlogopite, and note that phlogopite can, rarely, contain as much as 8 wt% fluorine under these conditions (e.g., Munoz 1984; Hensen and Osanai 1994; Dooley and Patiño Douce 1996; Motoyoshi and Hensen 2001; Trønnes 2002). The micas in meimechites have been described as biotite, not phlogopite, but their fluorine contents have not been measured.

Some petrologic estimates for water content required for mica stability are available, but there are no applicable low-pressure experiments on mica stability. Lange et al. (1993) made estimates of eruptive temperature for lavas from Mono Lake, CA from 1,025 to 1,172°C based on coexisting mineral pairs. Based on these temperatures, they estimate eruptive water contents from MELTs algorithm range from 1.7 to 2.7 wt%. Righter and Carmichael (1996) found that, depending upon the fluorine content, 3–6 wt% water may be required to stabilize phenocrystic mica in Mexican lamprophyres.

Equating the water required for mica stability with magmatic pre-eruptive water content is only correct if mica crystallized first. If 3–6 wt% of water is required but mica only crystallized after 50% or more of the lava was solidified, then the initial magmatic water content was at most 1.5–3 wt%. In meimechites the degree of lava crystallization before mica stability is unknown, but a significant fraction of olivine had crystallized first as indicated by the interstitial texture of the mica, and the fraction of olivine phenocrysts is in some cases 50% or higher. Using this line of reasoning and the range of olivine phenocryst fractions in meimechites, preeruptive water content for meimechites of 0.5–3 wt% may be a reasonable estimate.

Further unknowns in the stabilization of groundmass mica are the roles of carbon dioxide, sulfur, and fluorine. Some K-rich magmas (Ugandan kamafugites, Siberian meimechites, and Greenlandic lavas, for example) are associated with carbonatites and therefore carbon dioxide is a strong candidate volatile (Fedorenko and Czamanske 1997; Lloyd et al. 2002; Bernstein et al. 2000). Siberian meimechites are closely associated with the carbonatites, ijolites, ankaratrites, and phlogopite deposits of the Guli massif (Fedorenko and Czamanske 1997). Phlogopite is significantly stabilized by fluorine, lowering the water content required for stability, and fluorine is also a candidate atmospheric gas to participate in the contemporaneous global extinction, as is sulfur. However, Kamo et al. (2003) states that the Guli province is slightly more recent, perhaps the final event in the Siberian flood basalts, at 250.2 ± 0.3 Ma. The Guli carbonatites, therefore, postdate the Maymecha meimechites.

The apparently non-explosive eruptive styles of the meimechites may not significantly limit their pre-eruptive carbon dioxide contents. Explosive eruption occurs when exsolving bubbles cannot escape the rising magma quickly enough, and their growth drives the liquid phase violently upward. If bubbles can readily escape, explosive eruption is avoided. Carbonatite magmas, for example, can have effusive, Hawaiin-style eruptions. Meimechite magmas have exceptionally low viscosities due to their low fractions of tetrahedrally coordinated ions and their high magnesium contents, and may therefore successfully degas without explosive eruption (the difficulty of quenching these liquids to glass in experiments is testimony to their low viscosity). While low silica creates low viscosity and therefore aids in degassing, low silica also appears to chemically facilitate the retention of carbon dioxide in the magma. Papale (1999) finds that at 3 GPa an olivine nephelinite can contain 4–7 wt% CO_2, while a tholeiite can contain only about 1 wt%. At 0.5 kbar MORB CO_2 content has fallen to near zero, but a leucitite can contain about 0.5 wt% CO_2 at the same pressure.

Significant carbon dioxide content in the magma may drive fractionation by the temperature drop imposed upon the magma as carbon dioxide degasses, which would be limited by the degree of olivine fractionation apparent in the meimechites: about 50% (Fig. 3). High magma temperature also constrains degassing: a sufficiently high temperature will prevent rising, depressurizing magmas from intersecting the CO_2-added solidus, and allow it to retain more carbon dioxide to lower pressures (Lee et al. 2000; Wyllie and Ryabchikov 2000). The meimechite magma, then, may have retained as much as a half weight percent of CO_2 to the near-surface, and could have originated with a higher content without catastrophic degassing during upward migration, depending upon its temperature.

Lack of orthopyroxene stability and low silica content: implications for the magmatic source region

A primitive basaltic or picritic magma in equilibrium with mantle olivine is expected to have melted from a four-phase mantle peridotite containing olivine, clinopyroxene, orthopyroxene, and an aluminous phase. The unfractionated magma should be found experimentally to be in equilibrium with the four phases from which it melted. If melting had progressed to a high degree, the source might be missing clinopyroxene, but not orthopyroxene.

Meimechites are not alone in their lack of orthopyroxene saturation: while some K-rich magmas are in equilibrium with orthopyroxene (Esperanca and Holloway 1987; Edgar and Condliffe 1978; Edgar et al. 1980; Sato 1997; Carlier et al. 1997, the vast majority are far from orthopyroxene equilibrium (Esperanca and Holloway 1987; Righter and Carmichael 1996; Barton and Hamilton 1978, 1979; Edgar and Condliffe 1978; Edgar et al. 1980; Elkins-Tanton and Grove 2003).

The lack of orthopyroxene at multiple saturation might be explained by high temperatures that force the experiment above the pyroxene solvus, into a part of phase space where pigeonite is stable in preference to clinopyroxene with orthopyroxene. This argument cannot be used, however, at lower pressures and temperatures, and in fact no orthopyroxene crystallizes even at temperatures over 200°C beneath the liquidus at one atmosphere pressure. Additionally, no orthopyroxene has been found in the groundmass of any natural meimechite. The lack of orthopyroxene is therefore a robust characteristic of the composition being studied.

Two possibilities remain to explain the lack of orthopyroxene in the experiments. First, the magma may have melted from a source that did not contain orthopyroxene. Second, the lack of orthopyroxene in experiments is an artifact that would be remedied by the addition of carbon dioxide in the assembly.

Candidate sources without orthopyroxene include eclogite, and peridotite that has been metasomatized. Meimechites are unlikely to have originated from eclogite: eclogitic melts have higher silica and higher Ca/(Ca+Fe+Mg) (e.g., Hammouda 2003). Additionally, A.V. Sobolev (personal communication) has developed a methodology using Mn/Fe fractionation in olivines that can differentiate eclogitic from peridotitic melts, and with FeO/MnO rations below 65 and NiO(FeO/MgO) ratios below 0.10, the olivines in meimechites require a peridotitic source.

Many researchers state that silica-undersaturated alkaline magmas such as kimberlites and melilites (and presumably meimechites) can only be produced from mantle-based reactions including carbon dioxide (Eggler 1974; Wyllie and Huang 1975; Brey and Green 1977; Eggler 1978; Wendtland and Mysen 1980; Hirose 1997; Lee et al. 2000; Lee and Wyllie 2000; Wyllie and Ryabchikov 2000; Dasgupta et al. 2006). Hirose (1997) and Lee et al. (2000) state that with progressive melting at higher temperatures, partial melts of carbonated peridotite change from carbonatitic to silicic melts at about 200°C above the solidus, but they are characteristically silica-poor. They add that the only way to bring the silica contents of mantle melts to these low values in concert with low alumina is by dissolving carbon dioxide. Lee and Wyllie (2000) add that with greater depths of melting the Mg/Ca ratio rises: a high Mg/Ca ratio is a common characteristic of meimechites.

Numerous cratonal xenoliths have been found that contain olivine, phlogopite, and clinopyroxene, but no orthopyroxene (e.g., Erlank et al. 1987). This composition is a candidate source material for the meimechites. Unfortunately no mantle xenoliths associated with meimechites are yet known, so the hypothesis cannot be tested directly (as it was in the Sierra Nevada; see Elkins-Tanton and Grove 2003, and references therein).

Metasomatizing peridotite has been suggested to remove orthopyroxene. Menzies and Chazot (1995) identified three agents for peridotite metasomatism: (1) carbonate-rich melts, (2) silicate melts; and (3) aqueous fluids. These possibilities, of course, are not mutually exclusive; a hydrous, CO_2-bearing magma may also produce this result. Discriminating among these possibilities is hindered by contradictory experimental evidence. Research exists demonstrating that water will react with peridotite to remove orthopyroxene (Erlank et al. 1987), and other research exists to show that water increases the stability of orthopyroxene in peridotite (Wyllie and Sekine 1982; Wunder and Melzer 2003).

Multiple researchers (Dalton and Wood 1993; Wood et al. 1996; Lee and Wyllie 2000; Keppler et al. 2003; Francis 2003) find that peridotite metasomatism by carbon dioxide-bearing fluids destabilizes orthopyroxene. Wehrlites are postulated to be the result of reactions between carbonate-rich melts and orthopyroxene in host peridotites through the reaction

$$\text{liquid} + \text{orthopyroxene} \Leftrightarrow \text{olivine} + \text{clinopyroxene} + \text{vapor}$$

(Dalton and Wood 1993; Lee and Wyllie 2000). Dalton and Wood (1993) experimentally converted lherzolite to wehrlite by reaction with a dolomitic liquid. The resulting wehrlitic peridotite is a candidate source for meimechite magmas, and its production would have released CO_2 vapor.

In possible contradiction, the presence of carbon dioxide has been shown in multiple studies to stabilize orthopyroxene (Edgar and Condliffe, 1978, Edgar et al. 1980; Sato 1997; Hirose 1997; Dalton and Presnall 1998) and to stabilize both orthopyroxene and garnet in others (Brey and Green 1977; Adam 1988). This argument is used to explain the lack of orthopyroxene in experiments: the lack of carbon dioxide in the

experimental assembly eliminates the orthopyroxene stability that existed in the carbonated source. Addition of carbon dioxide to the experiment should then stabilize orthopyroxene (but contrast with Nicholls and Whitford 1983, whose experiments on a high-potassium lava composition did not saturate with orthopyroxene even with up to 10 wt% added orthopyroxene and CO_2 completely replacing water). These arguments can be used with meimechites only if addition of carbon dioxide to experimental assemblages stabilizes orthopyroxene as well as garnet. Experiments with carbon dioxide and with mixed volatiles will be forthcoming.

The source for meimechite magmas is therefore likely to have been a peridotite metasomatized by carbon dioxide-bearing fluids. Several researchers have suggested a multi-stage process for creating silica-undersaturated alkali basalts from such a source (Wyllie and Huang 1975; Brey and Green 1977; Eggler 1978; Wendtland and Mysen 1980; Hammouda 2003): carbonates in downgoing slabs decompose at 2.5–3.5 GPa and release CO_2, which metasomatizes peridotite (Newton and Sharp 1975; Wyllie and Huang 1975; Yaxley et al. 1994). This metasomatized peridotite later melts to produce the undersaturated magmas.

Though the meimechite magma itself may not have been host to significant carbon dioxide, as discussed above, its likely source composition attests to voluminous carbon dioxide metasomatism. Therefore, the results of this study suggest that there may be a significant carbon dioxide association with the meimechites of the Siberian flood basalts.

Effects of volatile content on multiple saturation depth and temperature

Though we hypothesize that the bulk of volatiles metasomatizing the meimechite source region had escaped before melt generation, some trace volatiles were likely inherited by the magma. If the meimechite primary magma contained more water or carbon dioxide, then its true multiple saturation pressure and temperature will differ from those measured here, ~5.5 GPa and 1,700°C with ~1 wt% water. Researchers are in agreement that additions of water or carbon dioxide lower the temperature of multiple saturation. A variety of researchers have investigated the effects of water on the temperature of the liquidii pertinent to peridotite melting, and thus to multiple saturation. Water contents of 5–6 wt% have been shown by a variety of researchers to lower the temperature of multiple saturation point by 100–200°C when compared to the dry value, meaning a temperature depression of 10–40°C per weight percent of added water (Baker et al. 1994; Righter and Carmichael 1996; Sato 1997; Gaetani and Grove 1998). Gudfinnsson and Presnall (2002) find a somewhat larger effect of water on solidus temperature: 25–60°C per weight percent of water. The effect of water on temperature of melting is much more profound than its effect on pressure. Experiments presented in Sato (1997) show the pressure of melting is increased by about 0.15 GPa per percent of water in the melt.

The effect of carbon dioxide on melting temperature is more dramatic. Dalton and Presnall (1998) and Gudfinnsson and Presnall (2005) demonstrate as much as a 500°C drop between the dry and carbonate-bearing solidii for lherzolites and for the CMAS-CO_2 systems. Arndt et al. (1998) also noted that CO_2 might be an important consideration in the formation of meimechites, and estimated that its addition might lower the temperature of melting by 200 but suggested that the melting depth might be shallower as well.

Sobolev et al. (1991) found only traces of carbon dioxide and very little water in the ten meimechite melt inclusions measured. Even if carbon dioxide was as extensively involved in meimechite petrogenesis as this work suggests, little would be expected to be found in melt inclusions: Sobolev and Slutskii (1984) demonstrated by measuring pressure in olivine fluid inclusions that olivine fractionation occurred primarily in the 0.5–1.5 kbar interval and at high temperature, so much of the carbon dioxide should have been degassed before fluid was trapped in the olivines. Application of the QUILF method to olivines and their inclusions in this study produces a similar pressure range of crystallization. Because magmas would have largely devolatilized by these depths, in the absence of extensive additional experimental work, the original CO_2 content of the meimechites can only be estimated indirectly.

We suggest that meimechite bulk compositions, mineral phases, and the phases of multiple saturation are consistent with initial compositions including 0.5–3 wt% H_2O and an undefined quantity of CO_2. The initial volatile load may therefore be comparable to the experimental powder, or it may have been higher. A volatile load of 2 wt% water and 0.5 wt% CO_2, for example, would lower the magma's multiple saturation point by perhaps 100–150°C, as a rough estimate, lowering its temperature to ~1,550–1,600°C. Though still unusually hot, these are perhaps more likely temperatures for a thermal upwelling than was the 1,700°C figure obtained through experiments with ~1 wt% water. This volatile load would raise the pressure of multiple saturation by perhaps 0.2–0.5 GPa to 5.7–6.0 GPa.

Comparison of multiple saturation pressure and lithospheric thickness estimates

Because the meimechite magma was apparently formed from a hot mantle source and not by directly melting lithosphere, the pressure of multiple saturation supplies a maximum thickness for the lithosphere at the time of magma formation. The meimechite primary magma was last in contact with its source at a pressure of about 5.5 GPa, indicating that the relevant portion of the Siberian lithosphere was no thicker than ~175 km.

The Siberian craton, through which the basalts were erupted, was assembled in the Archaean. Archaean cratons studied today with tomography possess stiff, buoyant roots reaching 250–300 km into the mantle (Egorkin et al. 1987; Priestley and Debayle 2003). The relative shallowness of formation of the meimechites may indicate that the craton was thinned by the process of flood basalt formation. Numerical models of mantle plumes indicate that they cannot efficiently erode lithosphere (Moore et al. 1999), so another mechanism is needed. The current lithospheric thickness under the Siberian flood basalts is about 300 km (Egorkin et al. 1987; Priestley and Debayle 2003). The lithosphere therefore appears to have thinned to 175 km during flood basalt production, and then thickened to 300 km in the last 250 million years, perhaps aided by the addition of buoyant residuum of melting.

Elkins-Tanton and Hager (2000) suggested that the lower lithosphere under Siberia was destabilized by melt injection from a thermal upwelling, and that portions of the lower lithosphere sank as gravitational instabilities. An instability can create both the subsidence seen throughout the 3.5-km section of volcanics at Noril'sk (Czamanske et al. 1998) and thin the lithosphere, increasing the melting column.

At the time of the Siberian flood basalts the craton was surrounded by subduction zones (Nikishin et al. 2002; Torsvik and Cocks 2004). We suggest that the volatiles released during subduction metasomatized the mantle lithosphere, lending it an enriched trace element signature, high alkalis, and a significant volatile content. A sinking lithospheric instability can devolatilize as it sinks, just as a sinking slab does at a subduction zone (Elkins-Tanton 2005, 2006). Rising volatiles may metasomatize surrounding mantle material, producing an appropriate source for the meimechites along with a lithosphere thin enough to produce their relatively low-pressure signature. Alternatively, the surrounding upper mantle may have been previously metasomatized (as suggested by Carlson et al. 2006) and was able to melt adiabatically following the sinking of a gravitationally unstable material from the lithosphere (Elkins-Tanton and Hager 2000).

Conclusion

The final magmas of the Siberian flood basalts are volatile- and alkali-rich high-magnesium lavas called meimechites. This experimental study on a candidate primary meimechite magma containing ~1 wt% water indicates it originated at about 5.5 GPa and 1,700°C. The low pressure of formation indicates that the Siberian craton was significantly thinner at the time, and the high temperature supports formation in a thermal upwelling.

Both the complete absence of orthopyroxene in these experiments and the close association of natural meimechites with carbonatites suggest that the magma likely originated from a source that had interacted with a carbon dioxide-rich fluid.

We suggest therefore that meimechite bulk compositions, mineral phases, and the phases of multiple saturation are consistent with initial volatile compositions including 0.5–3 wt% H_2O a lesser quantity of CO_2. The addition of these volatiles is likely to move the magma's multiple saturation point by perhaps 100–150°C, as a rough estimate, lowering its temperature to ~1,550–1,600°C. Though still unusually hot, these are perhaps more likely temperatures for a thermal upwelling than was the 1,700°C figure obtained through experiments with ~1 wt% water. This volatile load would raise the pressure of multiple saturation by perhaps 0.2–0.5 GPa, to 5.7–6.0 GPa.

A sinking lithospheric gravitational instability is a mechanism for transporting volatiles and lithospheric trace elements to 5.5 or 6 GPa. The mantle and lithosphere under Siberia had been fluxed by subduction fluids and so was likely rich in water and carbon dioxide. Melts from the thermal upwelling that initiated the flood basalts would heat and weaken the mantle lithosphere, making gravitational instabilities likely. Meimechites in Siberia may therefore be the result of foundering continental lithosphere into a hot upwelling such as a plume tail. The accompanying release of carbon dioxide (and probably significant fluorine and sulfur) may have contributed to the apparently contemporaneous end-Permian extinction.

Acknowledgments This study was supported by a grant from the National Science Foundation Petrology and Geochemistry program. The authors are very grateful for the support of and samples given by the American Museum of Natural History, Gerry Czamanske, Nick Arndt, and Valeri Fedorenko. The multi-anvil experiments were made possible by generous

contributions from the Institute of Meteoritics at the University of New Mexico, Albuquerque, and experiments at lower pressure through the generosity of Mac Rutherford and Yan Liang at Brown University. Rick Carlson, Gerry Czamanske, Valeri Fedorenko, Alexei Ivanov, and Alexander Polozov were kind enough to give close readings and helpful comments for improving the paper. Nick Arndt and Rebecca Lange provided thorough and constructive reviews.

References

Adam J (1988) Dry, hydrous, and CO_2-bearing liquidus phase relationships in the CMAS system at 28 kbar, and their bearing on the origin of alkali basalts. J Geol 96:709–719

Agee CB, Li J, Shannon MC, Circone S (1995) Pressure–temperatures phase diagram for the Allende Meteorite. J Geophys Res B 100:17725–17740

Anderson DJ, Lindsley DH, Davidson PM (1993) QUILF: a PASCAL progrfam to assess equilibria among Fe–Mg–Ti oxides, pyroxenes, olivines, and quartz. Comput Geosci 19:1333–1350

Arndt NT, Christiansen U (1992) The role of lithospheric mantle in continental flood volcanism: thermal and geochemical constraints. J Geophys Res 97:10967–10981

Arndt NT, Lehnert K, Vasil'ev YR (1995) Meimechites: highly magnesian lithosphere-contaminated alkaline magmas from deep subcontinental mantle. Lithos 34:41–59

Arndt NT, Chauvel C, Czamanske G, Fedorenko V (1998) Two mantle sources, two plumbing systems: tholeiitic and alkaline magmatism of the Maymecha River basin, Siberian flood volcanic province. Contrib Miner Petrol 133:297–313

Baker MB, Grove TL, Price R (1994) Primitive basalts and andesites from the Mt Shasta region, N California: products of varying melt fraction and water content. Contrib Miner Petrol 118:111–129

Barton M, Hamilton DL (1978) Water-saturated melting relations of 5 kilobars of three Leucite Hills lavas. Contrib Miner Petrol 66:41–49

Barton M, Hamilton DL (1979) The melting relationships of a madupite from the Leucite Hills, Wyoming, to 30 kb. Contrib Miner Petrol 69:133–142

Basu AR, Poreda RJ, Renne PR, Teichmann F, Vasilev YR, Sobolev NV, Turrin BD (1995) High-^{3}He plume origin and temporal–spatial evolution of the Siberian flood basalts. Science 269:822–825

Beane JE, Turner CA, Hooper PR, Subbarao KV, Walsh JN (1988) Stratigraphy, composition and form of the Deccan basalts, Western Ghats. India Bull Volcanol 48(1):61–83

Bernstein S, Leslie AG, Higgins AK, Brooks CK (2000) Tertiary alkaline volcanics in the Nunatak Region, Northeast Greenland: new observations and comparison with Siberian maymechites. Lithos 53:1–20

Brey G, Green DH (1977) Systematic study of liquidus relations in olivine melilitite + H_2O + CO_2 at high pressures and petrogenesis of an olivine melilitite magma. Contrib Miner Petrol 61:141–162

Campbell IH, Czamanske GK, Fedorenko VA, Hill RI, Stepanov V (1992) Synchronism of the Siberian traps and the Permian–Triassic boundary. Science 258(5089):1760–1763

Carlier G, Lorand J-P, Audebaud E, Kienast J-R (1997) Petrology of an unusual orthopyroxene-bearing minette suite from southeastern Peru, Eastern Andean Cordillera: Al-rich lampriotes contaminated by peraluminous granites. J Volcan Geotherm Res 75:59–87

Carlson RW, Czamanske G, Ilupin I, Fedorenko V (2006) A comparison of Siberian meimechites and kimberlites: implications for the source of high-Mg alkalic magmas and flood basalts. G-cubed (in press)

Chung S-L, Jahn BM (1995) Plume–lithosphere interaction in generation of the Emeishan flood basalts at the Permian–Triassic boundary. Geology 23:889–892

Czamanske GK, Gurevitch AB, Fedorenko V, Simonov O (1998) Demise of the Siberian plume: Paleogeographic and paleotectonic reconstruction from the prevolcanic and volcanic record, North-central Siberia. Int Geol Rev 40:95–115

Dalrymple GB, Czamanske GK, Fedorenko VA, Simonov ON, Lanphere MA, Likhachev AP (1995) A reconnaissance ^{40}ar/^{39}ar geochronologic study of ore-bearing and related rocks, Siberian Russia. Geochim Cosmochim Acta 59:2071–2083

Dalton JA, Presnall DC (1998) Carbonatitic melts along the solidus of model lherzolite in the system CaO–MgO–Al_2O_3– SiO_2– CO_2 from 3 to 7 GPa. Contrib Miner Petrol 131:123–135

Dalton JA, Wood BJ (1993) The compositions of primary carbonate melts and their evolution through wallrock reaction in the mantle. Earth Planet Sci Lett 119:511–515

Dasgupta R, MM Hirschmann, K Stalker (2006) Immiscible transition from carbonate-rich to silicate-rich melts in the 3 GPa melting interval of eclogite + CO_2 and genesis of silica-understaurated ocean island lavas. J Pet 47(4):647–671

Dobretsov NL, Vernikovsky VA (2001) Mantle plumes and their geologic manifestations. Int Geol Rev 43:771–787

Dooley DF, AE Patiño Douce (1996) Fluid-absent melting of F-rich phlogopite + rutile + quartz. Am Min 81:202–212

Edgar AD, Condliffe E (1978) Derivation of K-rich ultramafic magmas from a peridotitic mantle source. Nature 275:639–640

Edgar AD, Condliffe E, Barnett RL, Shirran GJ (1980) An experimental study of an olivine ugandite magma and mechanisms for the formation of its K-enriched derivatives. J Pet 21:475–497

Eggler DH (1974) Effect of CO_2 on the melting of peridotite. Carnegie Inst Wash Year Book 72:457–467

Eggler DH (1978) The effect of CO_2 upon partial melting of peridotite in the system Na_2O–CaO–Al_2O_3–MgO–SiO_2–CO_2 to 35 kb, with an analysis of melting in a peridotite–H_2O–CO_2 system. Am J Sci 287:305–343

Egorkin AV, Zuganov SK, Pavlenkova NA, Chernyshov NM (1987) Results of lithospheric studies from long-range profiles in Siberia. Tectonophysics 140:29–47

Elkins-Tanton LT (2005) Continental magmatism caused by lithospheric delamination. In: Foulger GR, Natland JH, Presnall DC, Anderson DL (eds) Plates, plumes, and paradigms. Geological Society of America, New York, pp. 449–461

Elkins-Tanton LT (2006) Continental magmatism, volatile recycling, and a heterogeneous mantle caused by lithospheric gravitational instabilities. J Geophys Res (in press)

Elkins Tanton LT, Hager BH (2000) Melt intrusion as a trigger for lithospheric foundering and the eruption of the Siberian flood basalt. Geophys Res Lett 27:3937–3940

Elkins-Tanton LT, Grove TL (2003) Evidence for deep melting of hydrous, metasomatized mantle: Pliocene high potassium magmas from the Sierra Nevadas. J Geophys Res 108: 2350, DOI 101029/2002JB002168

Elkins-Tanton LT, Chatterjee N, Grove TL (2003) Experimental and petrological constraints on lunar differentiation from the Apollo 15 green picritic glasses. Met Planet Sci 38:515–527

Erlank AJ, Waters FG, Hawkesworth CJ, Haggerty SE, Allsopp HL, Rickard RS, Menzies M (1987) Evidence for mantle metasomatism in peridotite nodules from the Kimberley Pipes, South Africa. In: Menzies MA, Hawkesworth CJ (eds) Mantle metasomatism. Academic, New York, pp 221–311

Esperanca S, Holloway JR (1987)On the origin of some mica-lamprophyres: experimental evidence from a mafic minette. Contrib Miner Pet 95:207–216

Fedorenko VA, Czamanske GK (1997) Results of new field and geochemical studies of the volcanic and intrusive rocks of the Maymecha-Kotuy area, Siberian flood-basalt province, Russia. Int Geol Rev 39:479–531

Fedorenko VA, Lightfoot PC, Naldrett AJ, Czamanske GK, Hawkesworth CJ, Wooden JL, Ebel DS (1996) Petrogenesis of the flood-basalt sequence at Noril'sk, North-central Siberia. Int Geol Rev 38:99–135

Francis D (1995) The implications of picritic lavas for the mantle sources of terrestrial volcanism. Lithos 34:89–105

Francis D (2003) Implications of major element composition for the mantle sources of kimberlite, aillikite, olivine lamprophyre and meimechite. 8th International Kimberlite Conference long abstract

Gaetani GA, Grove TL (1998) The influence of water on melting of mantle peridotites. Contrib Miner Petrol 131:323–346

Gibson SA, Thompson RN, Leonardos OH, Dickin AP, Mitchell JG (1999) The limited extent of plume–lithosphere interactions during continental flood-basalt genesis: geochemical evidence from Cretaceous magmatism in southern Brazil. Contrib Miner petrol 137(1–2):147–169

Gudfinnsson GH, Presnall DC (2002) The minimum potential temperature of the Hawaiian mantle is about 1420C. Eos Trans AGU 83 (47) Fall Meeting Suppl Abstract V52D-06

Gudfinnsson GH, Presnall DC (2005) Continuous gradations among primary carbonatitic, kimberlitic, melilitic, basaltic, picritic, and komatiitic melts in equilibrium with garnet lherzolite at 3–8 GPa. J Pet: DOI 101093/petrology/egi029

Hammouda T (2003) High-pressure melting of carbonated eclogite and experimental constraints on carbon recycling and storage in the mantle. Earth Planet Sci Lett 214:357–368

Hawkesworth CJ, Lightfood PC, Fedorenko VA, Blake S, Naldrett AJ, Doherty W, Gorbachev NS (1995) Magma differentiation and mineralisation in the Siberian flood basalts. Lithos 34:61–88

Hensen BJ, Osanai Y (1994) Experimental study of dehydration melting of F-bearing biotite in model pelitic compositions. Miner Mag 58A:410–411

Herzberg C, O'Hara MJ (2002) Plume-associated ultramafic magmas of Phanerozoic age. J Pet 43:1857–1883

Hirose K (1997) Partial melt compositions of carbonated peridotite at 3 GPa and role of CO_2 in alkali-basalt magma generation. Geophy Res Lett 24:2837–2840

Hooper PR, Hawkesworth CJ (1993) Isotopic and geochemical constraints on the origin and evolution of the Columbia River Basalt. J Pet 34:1203–1246

Ivanov AV, Rasskazov SV, Feoktistov GD, He H, Boven A (2005) $^{40}Ar/^{39}Ar$ dating of Usol'skii sill in the south-eastern Siberian Traps Large Igneous Province: evidence for the long-lived magmatism. Terra Nova 17:203–208 DOI 101111/j1365–3121200400588x

Kamo SL, Czamanske GK, Krough TE (1996) A minimum U–Pb age for Siberian flood basalt volcanism. Geochim Cosmochim Acta 60:3505–3511

Kamo SL, Czamanske GK, Amelin Y, Fedorenko VA, Davis DW, Trofimov VR (2003) Rapid eruption of Siberian flood-volcanic rocks and evidence for coincidence with the Permian–Triassic boundary and mass extinction at 251 Ma. Earth Planet Sci Lett 214(1–2):75–91

Kazanskii AY, Kazanskii YP, Saraev SV, Moskvin VI (2000) The Permo–Triassic boundary in volcano sedimentary section of the West-Siberian plate according to paleomagnetic data (from studies of the core from the Tyumenskaya superdeep borehole SD-6). Geol Geofizika 41:327–339

Keppler H, Wiedenbeck M, Shcheka SS (2003) Carbon solubility in olivine and the mode of carbon storage in the Earth's mantle. Nature 424:414–416

Kogarko LN, Ryabchikov ID (1995) Geochemical data on conditions of Meymechite-magma generation in polar Siberia. Geochem Int 33(11):119–130

Lange RA, Carmichael ISE, Renne PR (1993) Potassic volcanism near Mono basin, California: evidence for high water and oxygen fugacities inherited from subduction. Geology 21:949–952

Le Bas MJ (2000) IUGS reclassification of the high-Mg and picritic volcanic rocks. J Pet 41(10):1467–1470

Lee WJ, Wyllie PJ (2000) The system $CaO–MgO–SiO_2–CO_2$ at 1 GPa, metasomatic wehrlites, and primary carbonatite magmas. Contrib Miner Petrol 138:214–228

Lee WJ, Huang WL, Wyllie P (2000) Melts in the mantle modeled in the system $CaO – MgO – SiO_2 – CO_2$ at 27 GPa. Contrib Miner Petrol 138:199–213

Lightfood PC, Naldrett AJ, Gorbachev NS, Doherty W, Fedorenko VA (1990) Geochemistry of the Siberian trap of the Noril'sk area, USSR, with implications for the relative contributions of crust and mantle to flood basalt magmatism. Contrib Mineral Petrol 104:631–644

Lloyd FE, Wooley AR, Stoppa F, Eby GN (2002) Phlogopite–biotite paragenses from the K-mafic-carbonatite effusive magmatic association of Katwe-Kikorongo, SW Uganda. Miner Pet 74:299–322

Mahoney JJ, Macdougall JD, Lugmair GW, Gopalan K, Krishnamurthy P (1985) Origin of contemporaneous tholeiitic and K-rich alkaliv lavas: a case study from the northern Deccan Plateau, India. Earth Planet Sci Lett 72(1):39–53

Masaitis VL (1983) Permian and Triassic volcanism of Siberia, Zapiski VMO, part CXII, issue 4:412–425 (in Russian)

Menzies MA, Chazot G (1995) Fluid processes in diamond to spinel facies shallow mantle. J Geodyn 20:387–415

Milanovskiy YY (1976) Rift zones of the geologic past and their associated formations. Report 2. Int Geol Rev 18:619–639

Mohr P, Zanetton B (1988) The Ethiopian flood basalt province. In: Macdougall JD (ed) continental flood basalts. Kluwer, Dordrecht, pp 63–110

Moore WB, Schubert G, Tackley PJ (1999) The role of rheology in lithospheric thinning by mantle plumes. Geophys Res Lett 26:1,073–1,076

Motoyoshi Y, Hensen BJ (2001) F-rich phlogpite stability in ultra-high-temperature metapelites from the Napier Complex, East Antarctica. Am Miner 86:1404–1413

Munoz JL (1984) F–OH and Cl–OH exchange in micas with applications to hydrothermal ore deposits. In: Bailey SW (eds) Micas. Reviews in Mineralogy 13. Mineralogical Association of America, Washington, pp 469–493

Newton RC, Sharp WE (1975) Stability of forsterite + CO_2 and its bearing on the role of CO_2 in the mantle. Earth Planet Sci Lett 26:239–244

Nicholls IA, Whitford DJ (1983) Potassium-rich volcanic rocks of the Muriah complex, Java, Indonesia: products of multiple magma sources? J Volcan Geo Res 18:337–359

Nikishin AM, Ziegler PA, Abbott D (2002) Permo-Triassic intraplate magmatism and rifting in Eurasia: implications for

mantle plumes and mantle dynamics. Tectoniphysics 351(1–2):3–39

Papale P (1999) Modeling of the solubility of a two=component H_2O + CO_2 fluid in silicate liquids. Am Min 84:477–492

Piccirillo EM (1988) Continental flood volcanism from the Parana basin (Brazil). In: Macdougall JD (eds) continental flood basalts. Kluwer, Dordrecht, pp 195–238

Priestley K, Debayle E (2003) Seismic evidnce for a moderately thick lithosphere beneath the Siberian platform. Geophys Res Lett 30(3):1118, DOI 101029/2002GL015931

Reichow MK, Saunders AD, White RV, Pringle MS, Al'Mukhamedov AI, Medvedev AI, Kirda NP (2002) Ar-40/Ar-39 dates from the West Siberian Basin: Siberian flood basalt province doubled. Science 296:1846–1849

Renne PR, Basu AR (1991) Rapid eruption of the Siberian Traps flood basalts at the Permo-Triassic boundary. Science 253(5016):176–179

Righter K, Carmichael ISE (1996) Phase equilibria of phlogopite lamprophyres from western Mexico: biotite-liquid equilibria and *P–T* estimates for biotite-bearing igneous rocks. Contrib Miner Petrol 123:1–21

Ross P-S, Ukstins Peate I, McClintock MK, Xu YG, Skilling IP, White JDL, Houghton BF (2005) Mafic volcaniclastic deposits in flood basalt provinces: a review. J Volcan Geotherm Res 145:281–314

Ryabov VV, Konenko VF, Khmelnikova OS (1985) Rock-forming minerals of picritic basalts of the Noril'sk region. Sov Geol Geophys 26(4):77–84

Sato K (1997) Melting experiments on a synthetic olivine lamproite composition up to 8 GPa: implications to its petrogenesis. J Geophys Res 102:14751–14764

Saunders AD, England RW, Reichow MK, White RV (2005) A mantle plume origin for the Siberian traps: uplift and extension in the West Siberian Basin, Russia. Lithos 79:407–424

Sheinmann Yu M (1947) New petrological province in trhe northern parts of the Siberian Platforms. Proc Russian Academy Sci Geological Series 3:15–28

Sobolev AV, Slutskii AB (1984) Composition and crystallization conditions of the initial melt of the Siberian meimechites in relation to the general problem of ultrabasic magmas. Geologiya I Geofizika 25(12):97–109

Sobolev AV, Kamenetskaya VS, Kononkova NN (1991) New data on petrology of Siberia meimechites. Geochem Int 8:1084–1095

Stewart K, Rogers N (1996) Mantle plume and lithosphere contributions to basalts from southern Ethiopia. Earth Planet Sci Lett 139:195–211

Torsvik TH, Cocks LRM (2004) Earth geography from 400 to 250 Ma: a palaeomagnetic, faunal and facies review. J Geol Soc 161:555–572

Trønnes RG (2002) Stability range and decomposition of potassic richterite and phlogopite end members at 5–15 GPa. Min Pet 74:129–148

Walderhaug HJ, EA Eide, RA Scott, S Inger, EG Golioko (2005) Palaeomagnetism and $^{40}Ar/^{39}Ar$ grochronology from the South Taimyr igneous complex, Arctic Russia: a Middle–Late Triassic magmatic pulse after Siberian flood-basalt volcanism. Geophys J Int 163:501–517

Wendtland RF, Mysen BO (1980) Melting phase relations of natural peridotite + CO_2 as a function of degree of partial melting at 15 and 30 kbar. Am Miner 65:37–44

Wood BJ, Pawley A, Frost DR (1996) Water and carbon in the Earth's mantle. Phil Trans: Math Phys Eng Sci 354(1711):1495–1511

Wooden JL, Czamanske GK, Fedorenko VA, Arndt NT, Chauvel C, Bouse RM, King B-SW, Knight RJ, Siems DF (1993) Isotopic and trace-element constraints of mantle and crustal contributions to Siberian continental flood basalts, Noril'sk area, Siberia. Geochim Cosmochim Acta 57:3677–3704

Wunder B, Melzer S (2003) Experimental evidence on phlogopitic mantle metasomatism induced by phengite dehydration. Eur J Miner 15:641–647

Wyllie PJ, Huang WL (1975) Peridotite, kimberlite, and carbonatite explained in the system CaO– MgO– SiO_2– CO_2. Geology 3:621–624

Wyllie PJ, Ryabchikov ID (2000) Volatile components, magmas, and critical fluids in upwelling mantle. J Pet 41:1195–1206

Wyllie PT, Sekine T (1982) The formation of mantle phlogopite in subduction zone hybridization. Contrib Mineral Petrol 79:375–380

Xu Y, Chung S-L, Jahn B-M, Wu G (2001) Petrologic and geochmeical constraints on the petrogenesis of Permian–Triassic Emeishan flood basalts in southwestern China. Lithos 58:145–168

Yaxley GM, Green DH, Klápová H (1994) The refractory nature of carbonate during partial melting of eclogite: evidence from high pressure experiments and natural carbonate-bearing eclogites. Min Mag A58:996–997

Zolotukhin VV, Al'Mukhamedov AI (1988) Traps of the Siberian platform In: continental flood basalts. In: Macdougall JD (ed) continental flood basalts. Kluwer, Dordrecht, pp 273–310

Zolotukhin VV, Allmukhamedov AI (1991) Basalts of the Siberian platform: occurrence conditions, chemical composition, formation mechanism. Tr Inst Geol Geofiz (Novosibirsk) 803:7–39